INT. J. REMOTE SENSING, 2000, VOL. 21, NO. 6 & 7, 1251–1277

Improvements in the global biospheric record from the Advanced Very High Resolution Radiometer (AVHRR)

N. Z. EL SALEOUS†‡, E. F. VERMOTE†‡, C. O. JUSTICE§, J. R. G. TOWNSHEND†‖, C. J. TUCKER‡ and S. N. GOWARD†

†Laboratory for Global Remote Sensing Systems, Department of Geography, University of Maryland, College Park, MD 20942, USA
‡NASA's Goddard Space Flight Center, Code 923, Greenbelt, MD 20771, USA
§Department of Environmental Sciences, University of Virginia, Charlottesville, VA 22903, USA
‖ Institute of Advanced Computing Studies, University of Maryland, College Park, MD 20742, USA

Abstract. Results are provided of a project to derive improved products from the National Oceanic and Atmospheric Administration (NOAA) Advanced Very High Resolution Radiometer (AVHRR) data record for land investigations. As part of this project, a prototype AVHRR processing system has been developed. This paper describes the different components of this system, which include radiometric in-flight vicarious calibration for the visible and near infrared channels, geometric correction and atmospheric correction as pre-processing steps. The processed data are then stored in a new intermediate data format, which enables flexible compositing approaches. The system generates surface reflectance and vegetation index products as well as new higher order products of reflectance at 3.75 μm and active fires. A comparison of a significant sample of data with widely used precursor AVHRR products is presented to evaluate the processing chain and the improvements it provides.

1. Introduction

NASA's Earth Observing System (EOS) Pathfinder program is aimed at developing improved long-term satellite data products for global change research (Justice and Townshend 1994, Maiden and Greco 1994). The Pathfinder approach is to select, by peer review, important long-term satellite data sets which would contribute to the study of global change to be processed using algorithms published in the open literature. The AVHRR is considered a primary source of long-term data for terrestrial monitoring (Townshend 1994). For example, AVHRR data are currently being used to monitor interannual variation in vegetation and changes in the length of growing season (Tucker *et al.* 1994, Myneni *et al.* 1997) and the extent of land cover at continental and regional scales (DeFries and Townshend 1994, Laporte *et al.* 1995, Loveland and Belward 1997).

An initial AVHRR Pathfinder product was developed at NASA's Goddard Space Flight Center (GSFC) and has processed 12 years of Global Area Coverage (GAC) data (James and Kalluri 1994). A subsequent related project was developed at the EROS Data Center (EDC) using a similar processing chain to provide global 1 km data acquired through the International Geosphere–Biosphere Programme (IGBP)

International Journal of Remote Sensing
ISSN 0143-1161 print/ISSN 1366-5901 online © 2000 Taylor & Francis Ltd
http://www.tandf.co.uk/journals/tf/01431161.html

Global 1 km Project (Eidenshink and Faundeen 1994, Townshend *et al.* 1994). Several improvements to these data sets were identified through ongoing research at the GSFC and the University of Maryland (UMD) (Justice and Townshend 1994). In 1996, a new Pathfinder project was initiated to transform published research results into a 'next generation' processing code which could be used on both 8 km and 1 km AVHRR data. This project, known as AVHRR Land Pathfinder II is nearing completion. This paper outlines the approach that was adopted for the design of the processing code.

The new code uses an improved calibration method and corrects the visible and near-infrared channels of AVHRR for atmospheric effects of Rayleigh scattering, ozone and water vapour absorption. The ozone concentration is extracted from daily measurements by the Total Ozone Mapping Spectrometer (TOMS), and the water vapour content and surface pressure are obtained from products generated by NASA/GSFC Data Assimilation Office (DAO). The processing system generates surface reflectance data from AVHRR channels 1, 2 and 3, brightness temperature from channels 3, 4 and 5, the Normalized Difference Vegetation Index (NDVI), an active fires product and quality control fields for every pixel that carry information about confidence in the generated products and cloud contamination. The data are binned without resampling and stored in an intermediate data format referred to as Level 2G (Wolfe *et al.* 1998), which enables flexible approaches to temporal compositing. A summary of major differences between the initial Pathfinder (Pathfinder I) code and the new code (Pathfinder II) is presented in table 1.

The ongoing evaluation activity of the AVHRR Land Pathfinder II processing system includes comparing the generated products with existing global data sets such as the 8 km 10-day composite global surface reflectance and NDVI data set generated through the AVHRR Land Pathfinder I project at NASA/GSFC (James and Kalluri 1994), the Land SUrface Reflectances (LASUR) which is a global weekly data set of surface reflectances and vegetation indices derived from the AVHRR Global Vegetation Index (GVI) time series for 1989 and 1990 (Berthelot *et al.* 1996),

Table 1. Major differences between the Pathfinder I and Pathfinder II processing chains.

Pathfinder I	Pathfinder II
Forward navigation	Inverse navigation
Visible and near-infrared calibration based on Rao (1993a)	Visible and near-infrared calibration based on Vermote and Kaufman (1995)
Use of Digital Elevation Model (DEM) to estimate surface pressure for Rayleigh correction	Use of DAO data and DEM to provide a better estimate of surface pressure
No correction for water vapour absorption	Water vapour content obtained from DAO is used for water vapour correction
Temporal compositing is performed by selecting pixels yielding maximum NDVI value	All observations covering a grid cell are stored in Level 2G format to facilitate the use of multiple compositing techniques (Maximum NDVI, Minimum Ch1, Maximum *T*4 or *T*5)
Cloud mask is generated but not used in the compositing process	Cloud mask is used in the compositing process to assign higher priority to clear pixels
Pixels with high solar zenith angle are set to a fill value	Pixels with high solar zenith angle are preserved and flagged as of inferior quality
	New higher order products such as fire and channel 3 reflectance are generated

and the $1° \times 1°$ FASIR-NDVI data set derived from the Global Inventory, Monitoring, and Modeling Studies (GIMMS) continental data sets (Sellers *et al.* 1994).

2. Methods and analysis

To develop the capability to improve algorithms for processing AVHRR data, there was a need to develop a processing system that was flexible and modular. Flexibility enables the processing of data with different configurations and options, such as turning on and off the atmospheric correction component, without recourse to modifying and rebuilding the code. Modularity allows the removal and addition of processing steps, as these are updated by subsequent research without major modifications to the source code.

The AVHRR Land Pathfinder II processing system was developed in a UNIX environment using the C programming language, it complies with ANSI standards to facilitate its porting to different platforms. The overall architecture of the system, presented in figure 1, shows the data flow between the different components. The different modules, which represent the different processing steps, are described in detail in the next sections.

The processing system requires AVHRR Level 1B data as input and can ingest either Global Area Coverage (GAC) or Local Area Coverage (LAC) data. The processing configuration and options are set by user-defined parameters. They include the position of the corners and centre of the geographic area to be mapped (area of interest), the size and resolution of images to be produced, the time period desired (period of interest), the type of visible calibration to be applied (pre-flight or vicarious), the calibration coefficients to be used and atmospheric corrections to be applied.

The AVHRR instrument flown onboard the afternoon NOAA platforms acquires observations in five different channels. The spectral ranges covered by each channel are: 0.58–0.68 μm for channel 1; 0.725–1.10 μm for channel 2; 3.55–3.93 μm for channel 3; 10.30–11.30 μm for channel 4; and 11.50–12.50 μm for channel 5 (Cracknell 1997). For the sake of simplicity in this paper we will refer to these channels by their numbers only.

2.1. *Ingest*

Ingest is the first module called after decoding the user's request and configuring the processing system in accordance with the request. The main goal of Ingest is to read, decode Level 1B input data and convert these data to an internal format used by all the different modules of the system.

This module automatically identifies the type of input media and uses the Terabit Memory (TBM) header which constitutes the first record in NOAA's Level 1B data files (Kidwell 1997) to determine the spacecraft identifier and type of data. It also uses the acquisition time of the first scan line to determine the intersection between the orbit being processed and the geographic area requested by the user. This operation is performed by a direct navigation (see §2.2) of the orbit edges (first and last instantaneous field of view (IFOV) in each scan-line), and it aims at reducing the amount of input data to ingest by only processing those scan lines which intersect the predefined geographic area.

A preliminary quality control (QC) is performed in this module which decodes NOAA QC bits included in Level 1B data (Kidwell 1997) and rejects the scan lines where the fatal flag is set. The scan lines are also rejected and the data is marked

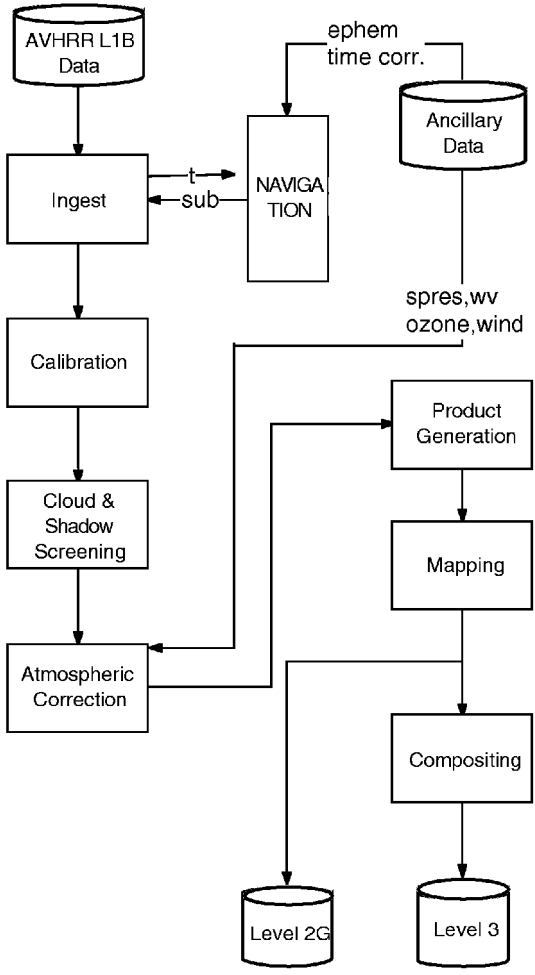

Figure 1. Overview of the AVHRR Land Pathfinder II processing system.

'bad'—e.g. if the acquisition time and date included in the data are invalid (day of year >366 for example). Other QC tests are included in the processing system after the radiometric calibration is applied to the data, where values that are outside of the expected range will lead to the pixel being considered 'unreliable'.

The spectral data and relevant telemetry data such as deep space and platinum resistor temperature (PRT) counts are decoded for valid scan lines and organized in orbital segment arrays that are passed to subsequent processing steps along with all necessary external ancillary data.

2.2. *Navigation*

Navigation is the procedure by which an Earth location is related to an IFOV. It can be performed in two distinct ways:

(1) forward (or direct) navigation, where for each IFOV, a geographic grid location is determined based on the scan acquisition time and the IFOV position in the scan, or

(2) inverse (or indirect) navigation, where for each grid cell of a predetermined geographic grid, the nearest IFOV scan number and position are determined.

The latter presents a clear advantage over the former because no data gaps due to sampling are present in the output product, since each grid cell is related to an IFOV, and secondly no geophysical biasing is introduced in the pixel selection (James and Kalluri 1994). The main disadvantage of the latter is the large requirement of CPU time due to the iterative nature of the method as described below.

For AVHRR Land Pathfinder II processing, we adopted an inverse navigation approach based on an iterative method developed at the University of Colorado (Rosborough *et al.* 1994). This approach utilizes satellite ephemeris information and an accurate orbital model that propagates the initial orbital elements to any time in the future. The accuracy of this procedure depends on several factors.

(1) *The accuracy of the ephemeris data which represent the initial position propagated by the orbital model.* These data are supplied daily by the Naval Space Surveillance Center (NAVSPASUR). The accuracy of the NAVSPASUR in ground track position is reported by Baldwin and Emery (1995) to be 0.5 km.
(2) *The accuracy of the orbital model used to propagate ephemeris data to the desired time.* A study by Baldwin and Emery (1995) shows that the ground track position error stays under 1 km if the ephemeris data used as initial orbital elements are younger than 2–3 days. Knowing that the ephemeris data are updated daily, the ground track position error due to uncertainties in the orbital model stays under 1 km.
(3) *The drift of the clock onboard the NOAA satellites which leads to a mis-synchronization between the satellite clock and the tracking station clock.* The error due to this factor can be significant. For NOAA-11 over the period 1991 to 1992, this error varied between -5 and 3 IFOVs (Baldwin and Emery 1995). Clock correction data for all of NOAA satellites used in this study were acquired from Jim Brown (Remote Sensing Laboratory, Rosentstiel School of Marine and Atmospheric Science, University of Miami).
(4) *The availability of attitude data consisting of roll, pitch and yaw.* Misalignment of the satellite/sensor axes introduce a significant error in the navigation process (a roll value of 0.001 radians correspond to a ground deviation of one IFOV). Roll, pitch and yaw values reported in the TIROS Information Processor (TIP) data stream are unreliable and should not be used in the navigation procedure (Brush 1982, Baldwin and Emery 1995). To reduce navigation errors, Ground Control Points (GCPs) have been used by several investigators (Ho and Asem 1986, Moreno and Melia 1993, Rosborough *et al.* 1994, Baldwin and Emery 1995). The method developed by Rosborough *et al.* (1994) and used by Baldwin and Emery (1995) presents the advantage of deriving attitude variation values that can be used *a priori* in the navigation procedure adopted by the AVHRR Land Pathfinder project. An illustration of the effect of the attitude correction is presented in figure 2, where the attitude variations derived by Baldwin and Emery (1995) were used in our navigation routines, when mapping images from South Africa (figure 2(*b*)) compared to the case where the attitude variations were ignored (figure 2(*a*)). A reference coastline map derived from NOAA's global, self-consistent, hierarchical, high-resolution shoreline database (GSHHS) (Wessel and Smith

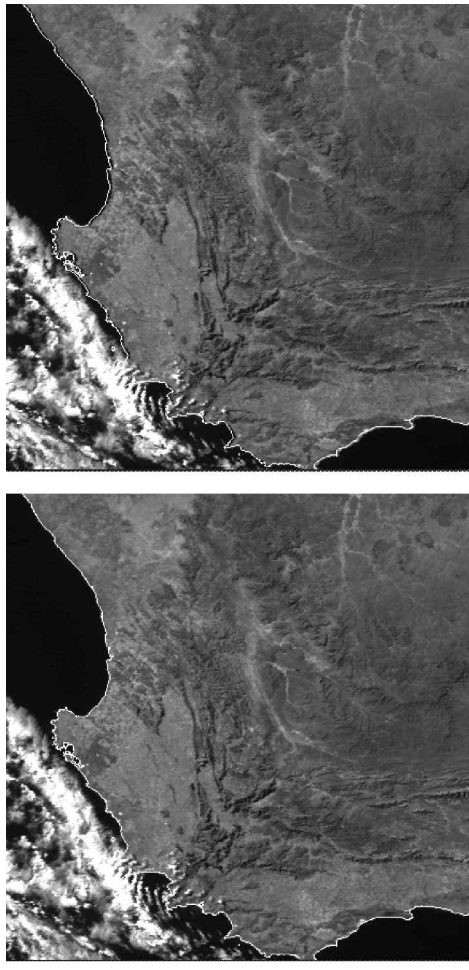

Figure 2. Illustration of attitude correction in the registration process. These two images show AVHRR near-infrared channel (870 nm) over South Africa for 5 May 1992. The roll, pitch and yaw were set to 0 in (*a*) and were set the values derived by Baldwin and Emery (1995) over Northern America in (*a*). The map outline overlayed on both images is derived from the NOAA GSHHS high-resolution vector shoreline data base.

1996) was overlaid on both images to help assess the improvement in navigation.

2.3. *Calibration*

2.3.1. *Visible and near-infrared*

Long term data sets require a stable well calibrated data record. Calibration of the visible and near infrared channels of the AVHRR has been problematic due to the lack of any onboard calibration (Holben *et al.* 1990, Teillet *et al.* 1990). The approach adopted here relies on calibration coefficients derived empirically from the data. The basic calibration equation to convert digital counts into a physical entity is

$$L_i = (DC_i - \text{offset}_i)G_i \tag{1}$$

where L_i is the normalized radiance, DC_i is the digital count delivered by the instrument for channel 1 or 2, offset_i is the digital count obtained when the instrument is viewing a black target and G_i is the gain for channel 1 or 2.

The offset_i value is obtained by averaging the deep space measurements available in each scan line. In an effort to reduce measurement noise, deep space counts are averaged over the whole orbital segment being processed, where we assume that the instrument performance does not vary. The value obtained is used for all the scan lines in that segment. Using the deep space view rather than a constant enabled us to obtain a better indication of instrument degradation. Figure 3 shows the daily averages of the deep space view for channels 1 and 2 over the lifetime of NOAA-9. A decrease of about 1% in the deep space count for channel 1 can be noticed over four years in the life of NOAA-9.

The sensor gain, G_i, is computed using the Vermote and Kaufman (1995) in-flight calibration method. The vicarious calibration approach implemented for this project uses AVHRR visible and near infrared data from the Pacific Ocean and present an improvement on what was originally published (Vermote and Kaufman 1995), by use of additional ancillary data sets including ozone concentration, water vapour content, surface pressure and wind speed and in employing a more reliable identification of cloud-free observations made possible by enhanced automatic processing and large volumes of input data. The standard deviation of the coefficients derived every nine days by this new technique reveals a high stability of the results and implies a precision of $\pm 0.5\%$ in the visible to near infrared ratio (figure 4) and $\pm 2\%$ in the degradation of the visible channel (figure 5). These results present an improvement on the values that were originally published (Vermote and Kaufman 1995) where the estimated precision of the ratio was $\pm 1\%$.

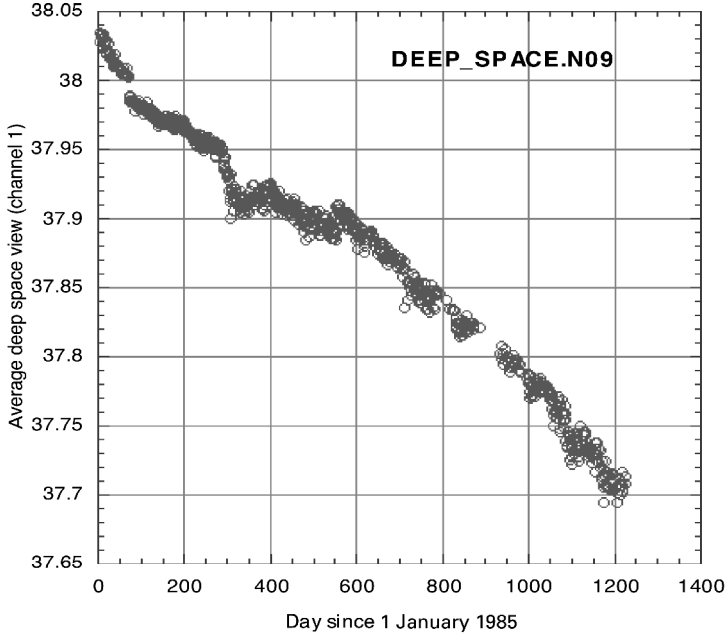

Figure 3. Deep space counts in NOAA-9 AVHRR red channel (670 nm) extracted from Level 1B data. It shows a decrease of about 1% over 4 years.

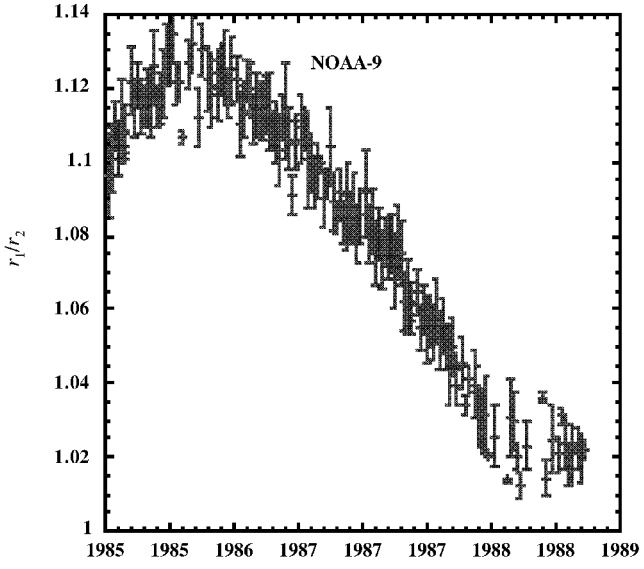

Figure 4. Visible to near-infrared ratio for NOAA-9 derived using the cloud calibration technique. The error bars represents the standard deviation of the derived ratio during a month and suggests a precision of ± 0.5%.

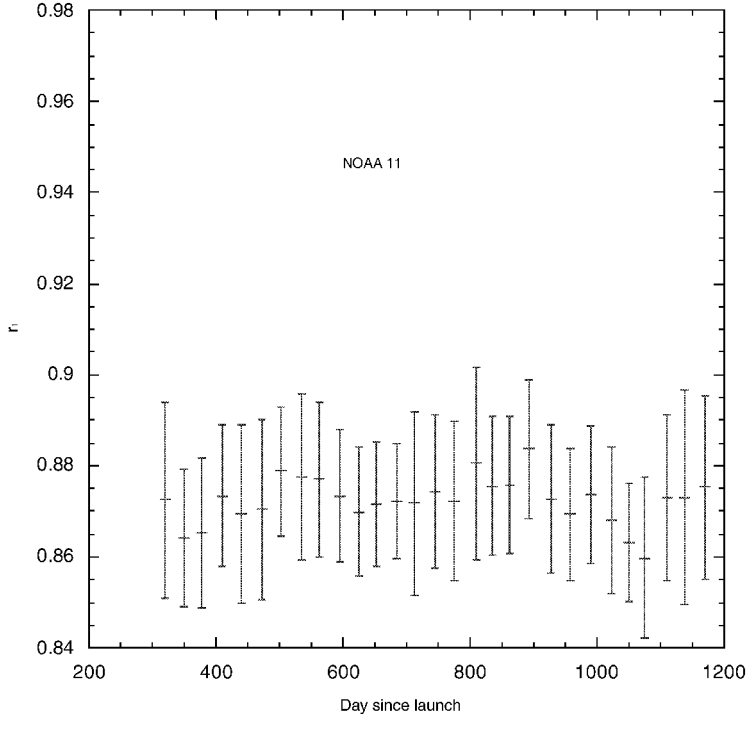

Figure 5. Degradation of NOAA-11 AVHRR visible channel computed by the ocean calibration technique. The error bars represents the standard deviation of the derived ratio during a month and suggests a precision of ± 2%.

This precision enables monitoring of the sensor degradation with time, confirming the good stability of NOAA-11 and the high rate of degradation of NOAA-9. Moreover, the high temporal frequency of the coefficients revealed by the technique shows that a linear/exponential degradation model, such as that used for the Pathfinder 1 data set as described by Rao (1993a) is a crude approximation of the degradation pattern both for single bands and band ratios. For band to band ratios, the improvements in the derived temporal variation is confirmed by analysis of data collected over the Sahara as shown in figure 6.

There remains residual uncertainty about the absolute calibration coefficients, due to a lack of knowledge of AVHRR characteristics such as linearity, polarization sensitivity and spectral band characterization. Previously published results suggested uncertainty in the spectral response, due to out-of-band response in the visible band, which was confirmed by a more in depth analysis of NOAA-14's AVHRR spectral band data and from independent measurements of AVHRR filters (Mekler 1994 Personal communication).

2.3.2. *Thermal calibration*

The infrared bands of the AVHRR (channels 3, 4 and 5) are calibrated onboard by using the measured radiation emitted by an internal calibration target (ICT) and deep space. The resultant computed radiances from channels 4 and 5 are then corrected for the nonlinear response of the HgCdTe detectors (Weinreb *et al.* 1990), following the recommendations of AVHRR Pathfinder Calibration Working Group (Rao 1993b, James and Kalluri 1994).

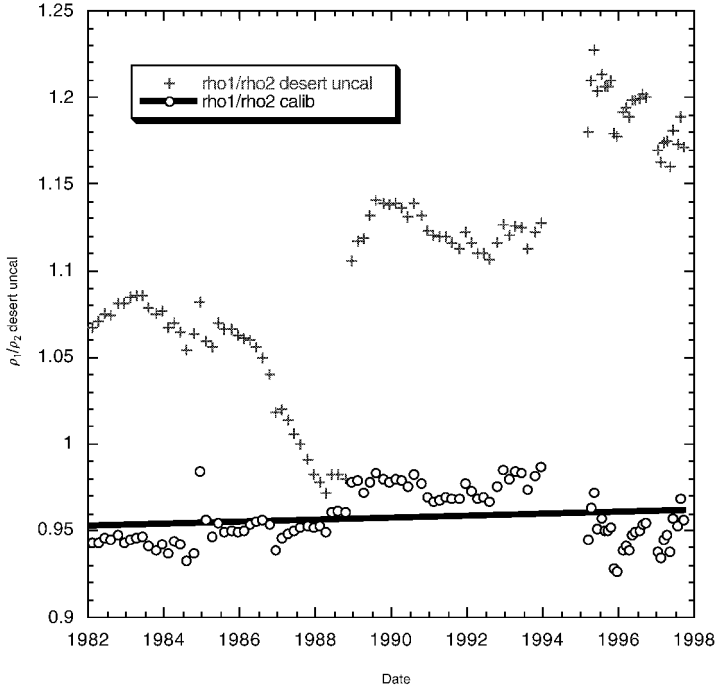

Figure 6. Visible/near-infrared reflectance ratio over desert using preflight (+) and in-flight (○) data for NOAA afternoon satellites.

2.4. *Cloud and shadow screening*

The cloud screening algorithm used in this study is based on the CLAVR algorithm (Stowe *et al.* 1991). It was applied to an array of 2×2 pixels and determines the property of this array as follows:

'cloudy', if all four pixels are determined to be cloudy by the algorithm;
'clear' if all the pixels are determined to be non-cloudy;
'mixed' otherwise.

The algorithm itself uses all five spectral bands of the AVHRR; it includes reflectance and thermal thresholds as well as reflectance and thermal uniformity tests. This algorithm was mainly developed for use with AVHRR GAC data, but is also applicable to LAC data. Our experience in using it with LAC data showed that the uniformity tests tend to flag clear pixels as cloudy which prompted us to turn them off when processing LAC data. Even though CLAVR is believed to overestimate the amount of clouds in some cases (Stowe *et al.* 1995, Simpson and Gobat 1996), it is an algorithm that can be applied globally. In our processing, data that are flagged cloudy or mixed are preserved and can be used in the compositing process (see §2.7), but are given a lower priority than cloud-free pixels.

The cloud shadow screening procedure used in this study aims at locating areas with potential cloud shadow contamination. Shadow screening is performed by a trigonometric computation as follows.

- Using the cloud mask generated earlier and the viewing geometry, determine the projection of the cloud on the ground.
- Estimate the cloud height using the difference in cloud top temperature and the surface temperature of cloud-free neighbouring pixels.
- Using solar geometry, compute the position that the cloud shadow will be cast.

The detected areas are then flagged and given lower priority in the compositing procedure than shadow-free pixels. An example of the cloud and cloud shadow mask produced by the system is presented in figure 7.

2.5. *Atmospheric correction*

Atmospheric scattering and absorption are known to affect the visible and near-infrared radiance reaching the satellite substantially (Tanré *et al.* 1992). These effects are also propagated to the NDVI, one of the most widely used products. Temporal compositing techniques such as the maximum NDVI were introduced to minimize atmospheric effects (Holben 1986). These techniques are of limited benefit for daily or short compositing periods, where atmospheric effects need taken account of, prior to using the data. Table 2 summarizes the magnitude of atmospheric effects on AVHRR bands 1 and 2 and on the NDVI. The numbers listed in this table were generated from simulations performed using the radiative transfer code known as the Second Simulation of the Satellite Signal in the Solar Spectrum (6S) (Vermote *et al.* 1997). We present here a scheme to correct for Rayleigh, ozone and water vapour effects and an approach to derive tropospheric aerosol optical thickness from AVHRR data. The effect of tropospheric aerosols is the most challenging factor to

Figure 7. Image (*b*) is cloud/cloud shadow mask produced by the system; grey areas are flagged as cloudy or mixed and white areas are cloud shadow. Image (*a*) is the near-infrared channel for the same area.

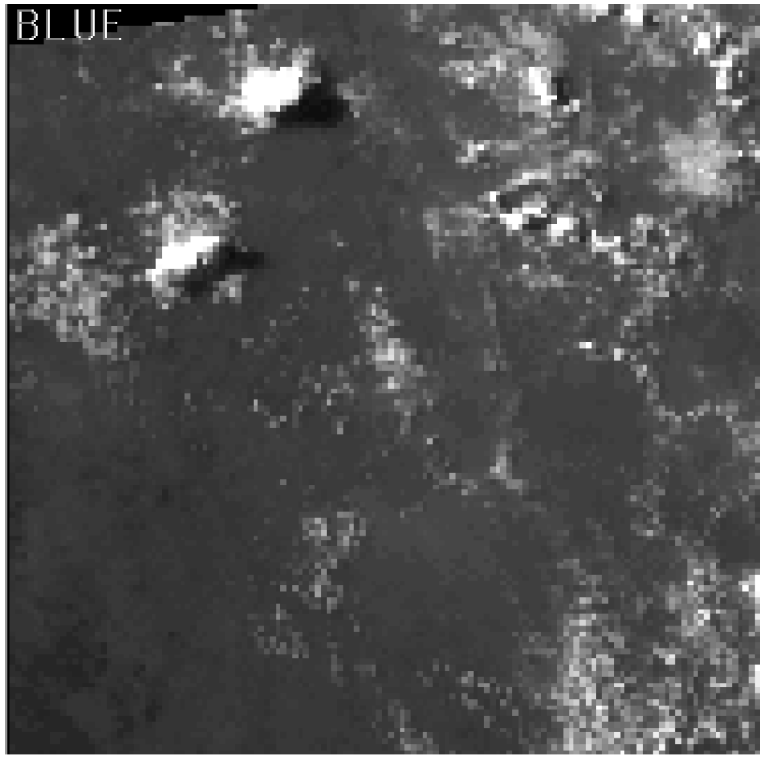

(a)

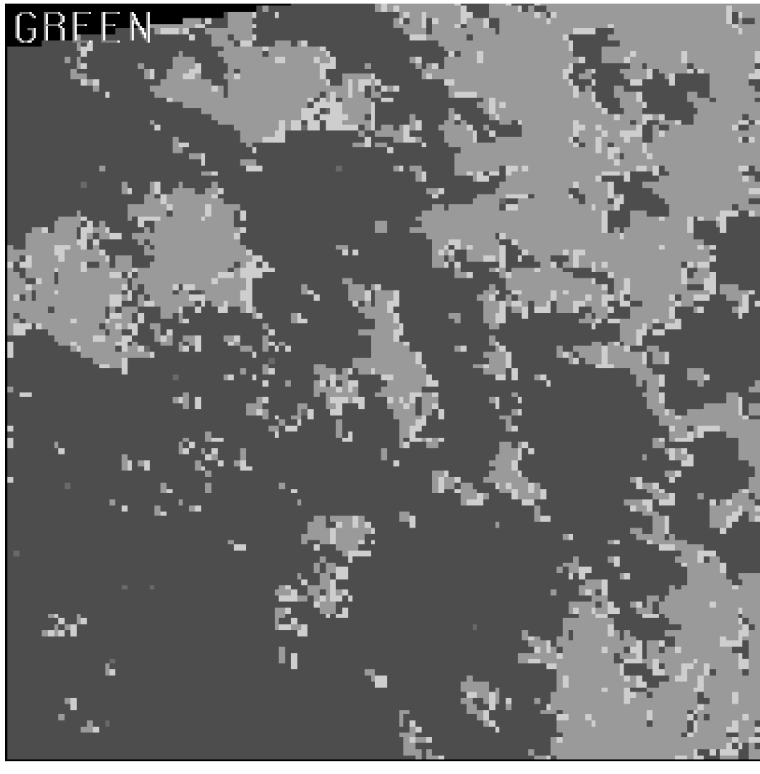

(b)

Table 2. Atmospheric effect on AVHRR data computed by the 6S radiative transfer code (Vermote *et al.* 1996).

	Ozone 0.247–0.48 (cm atm^{-1})	Water vapour 0.5–4.1 (g cm^{-2})	Rayleigh 1013 mb	Aerosol V: 60 km–10 km Continental
Channel 1	↘ 4.2% to 12%	↘ 0.7% to 4.4%	↗ 0.02 to 0.06	↗ 0.005 to 0.12
Channel 2	—	↘ 7.7% to 25%	↗ 0.006 to 0.02	↗ 0.003 to 0.083
NDVI (bare soil) $r_1 = 0.19$, $r_2 = 0.22$	↗ 0.02 to 0.06	↘ 0.011 to 0.12	↘ 0.036 to 0.094	↘ 0.006 to 0.085
NDVI (deciduous forest) $r_1 = 0.03$, $r_2 = 0.36$	↗ 0.006 to 0.017	↘ 0.036 to 0.038	↘ 0.086 to 0.23	↘ 0.022 to 0.035

correct, because of the spatial and temporal variability of these particles. The general equation for atmospheric correction for a Lambertian and uniform surface can be written (assuming no aerosols) as:

$$\rho_{TOA} = Tg_{O_3} Tg_{O_2} [\rho_R + T_R Tg_{H_2O} \rho_s / (1 - S\rho_s)] \quad (2)$$

where ρ_{TOA} is the top of the atmosphere reflectance, ρ_s is the surface reflectance, ρ_R is the Rayleigh atmospheric intrinsic reflectance, T_R is the Rayleigh transmittance, Tg_{O_2} is the oxygen transmittance, Tg_{O_3} is the ozone transmittance, Tg_{H_2O} is the water vapour transmittance and S is the Rayleigh spherical albedo.

2.5.1. *Rayleigh correction*

The Rayleigh reflectance, transmission and spherical albedo computation is based on analytical formulations developed by Vermote and Tanré (1992). This approach uses, as suggested by Chanderasekhar (1960), the quasi-isotropic behaviour of molecular scattering to develop an analytical expression of the atmospheric reflectance and uses a two-stream method corresponding to the Eddington approximation to describe the transmission function and compute the spherical albedo. This approach has the advantage of being fast enough to be implemented in a satellite data processing system and still meet accuracy requirements.

2.5.2. *Ozone correction*

Ozone molecules absorb a portion of the signal emitted towards the surface and reflected back towards the sensor. This effect, which is quantified by the ozone transmission function, is weak in AVHRR channel 2 but is non negligible in channel 1. The transmission function can be expressed mathematically as:

$$Tg_{O_3} = \exp(-amU_{O_3}) \quad (3)$$

where m *is* the air mass, U_{O_3} is the ozone concentration in (atm cm) and a is a wavelength dependent constant listed in table 3.

In the AVHRR Land Pathfinder II approach, U_{O_3} is obtained from the daily gridded ozone product derived from the Total Ozone Mapping Spectrometer

Table 3. Constants used in the atmospheric correction procedure.

	O_2 (a, b)	O_3 (a)	H_2O (a, b, c)	τ_r
Channel 1	0.0097904, 0.49207	0.057451	− 5.4136, 0.84205, 0.029284	0.052
Channel 2	0.0029896, 0.37584	0.00011516	− 3.4178, 0.68838, − 0.031404	0.019

(TOMS) which is generated by McPeters *et al.* (1993) and Herman *et al.* (1996) and distributed by the NASA/GSFC Data Active Archive Center (DAAC). The ozone concentrations derived from TOMS have several sources of uncertainties including errors in the measured radiance, parametrization of atmospheric parameters and physical input from laboratory measurements. These overall errors are divided into three categories: an absolute error of ± 3%, a random error of ± 2% and a time dependent error of ± 1.5% over 14 years (McPeters *et al.* 1996). TOMS data are available daily from the instrument onboard Nimbus-7 for the period of June 1979 to 6 May 1993, and from Meteor 3 for the period of November 1978 to December 1994 (Herman *et al.* 1996, McPeters *et al.* 1996). For the periods where TOMS data are unavailable, the ozone concentration was obtained from the Tiros Operational Vertical Sounder (TOVS) ozone product obtained from NOAA's National Centers for Environmental Predictions (NCEP) or alternatively from ozone climatology (London *et al.* 1976).

2.5.3. *Water vapour correction*

The measured signal is affected by water vapour in a similar way as by ozone. The water vapour transmission function is described mathematically as:

$$T_{H_2O} = \exp\{-\exp(a + b\log(mU_{H_2O}) + c[\log(mU_{H_2O})]^2\} \quad (4)$$

where m is the airmass, U_{H_2O} is the water vapour concentration in $g\,cm^{-2}$ and a, b and c are wavelength-dependent constants listed in table 3.

In the AVHRR Land Pathfinder II approach U_{H_2O} is obtained from the DAO diagnostics field (Schubert *et al.* 1993). Prior to using DAO data in our atmospheric correction process and in the absence of published accuracy for the water vapour product, we undertook an evaluation activity, comparing values obtained from the DAO with water vapour climatology (Oort 1983) and ground-based Sun photometer water vapour measurements. This showed good agreement between the DAO data and the photometer measurements, as shown in the example presented in figure 8, and led us to conclude that the DAO data set was adequate for water vapour correction.

2.5.4. *Tropospheric aerosol retrieval*

Recent research initiatives have been launched to measure and characterize aerosol distributions using a worldwide Sun photometer network (Holben *et al.* 1998). While measurements performed by this network provide an accurate and frequent estimate of aerosol optical thickness (AOT), they are local with a limited applicability for the generation of global data sets. In the AVHRR Land Pathfinder II project we estimate aerosol optical thickness from the AVHRR data set itself by

applying current knowledge of atmospheric effects on the measured signal and by assuming that the surface contribution is known. In the case of a clear ocean view outside of the Sun glint area, the surface reflectance in channels 1 and 2 of AVHRR is negligible (Vermote *et al.* 1996, Stowe *et al.* 1997). The observed signal is due mainly to the atmospheric contribution including aerosols. The observed reflectance in channels 1 and 2 is corrected for Rayleigh, ozone and water vapour effects, as described in earlier paragraphs, and the remaining signal, which should be due to aerosol scattering, is inverted using look-up tables to compute aerosol optical thickness in both channels. These look-up tables are generated using the 6S radiative transfer code for a rough ocean with a wind speed of $10\,m\,s^{-1}$ and for a maritime aerosol model. The look-up table computations were performed for ten aerosol optical depths varying from 0.05 to 2.0, for 22 solar and view zenith angles starting at 2.48° with a step of 3.71° and for 73 relative azimuth angles starting at 0° with a step of 2.5°. This approach cannot be applied consistently over land due to the dependency of the surface contribution on land cover and the invalid assumption that the surface contribution can be neglected. However, this approach can safely be used to derive optical thickness values over dark and dense vegetation targets where the surface contribution in channel 1 of AVHRR is low. To detect dark targets, we used the reflective part of channel 3 described in §2.2. The reflectance obtained from this channel is not affected by the atmosphere and provides a good estimate of the surface reflectance in channel 1. When this surface reflectance estimate is subtracted from the observed reflectance after correction for all other atmospheric effects, the remaining part, which is due to aerosols, is inverted to derive aerosol optical thickness using a look-up table similar to that used in the ocean inversion, with the exception of including a continental aerosol model.

As a demonstration of this approach, daily AVHRR data from 1989 and 1997 were used to derive aerosol optical thicknesses over ocean and dark land targets. The results were averaged and binned to a global $1° \times 1°$ grid similar to that shown in figure 9. An evaluation of the resulting optical thickness values was undertaken by comparing them to ground measurements obtained by Sun photometers. Retrieved versus measured values are plotted in figure 10 and show a good correlation between the values retrieved from AVHRR and ground measurements.

2.6. *Mapping and binning*

No single map projection will suit all user needs. For example, it is obvious that a polar projection is unsuitable for the study of tropical areas, and equatorial projections significantly distort polar areas. Hence it is clear that a selection of map projections is needed to satisfy the full spectrum of users. To offer a wide range of map projections to users, the AVHRR Land Pathfinder II code includes the General Cartographic Transformation Package (GCTP) map projection library available from the U.S. Geological Survey (USGS). This library offers over 20 choices of map projections and allows an individual setting all of the parameters that affect the shape and size of the output map (GCTP 1982). In addition to this feature, a tool to convert data from one projection to another has been implemented. Data from the orbit file are binned into the geographic grid using an inverse navigation approach which selects the nearest pixel to the centre of the grid cell. Only one orbit pixel can be binned to a given grid cell.

The gridding approach adopted for AVHRR Land Pathfinder II is a simplified version of the (Level 2 Grid (L2G)) adopted by the MODIS land group (Justice

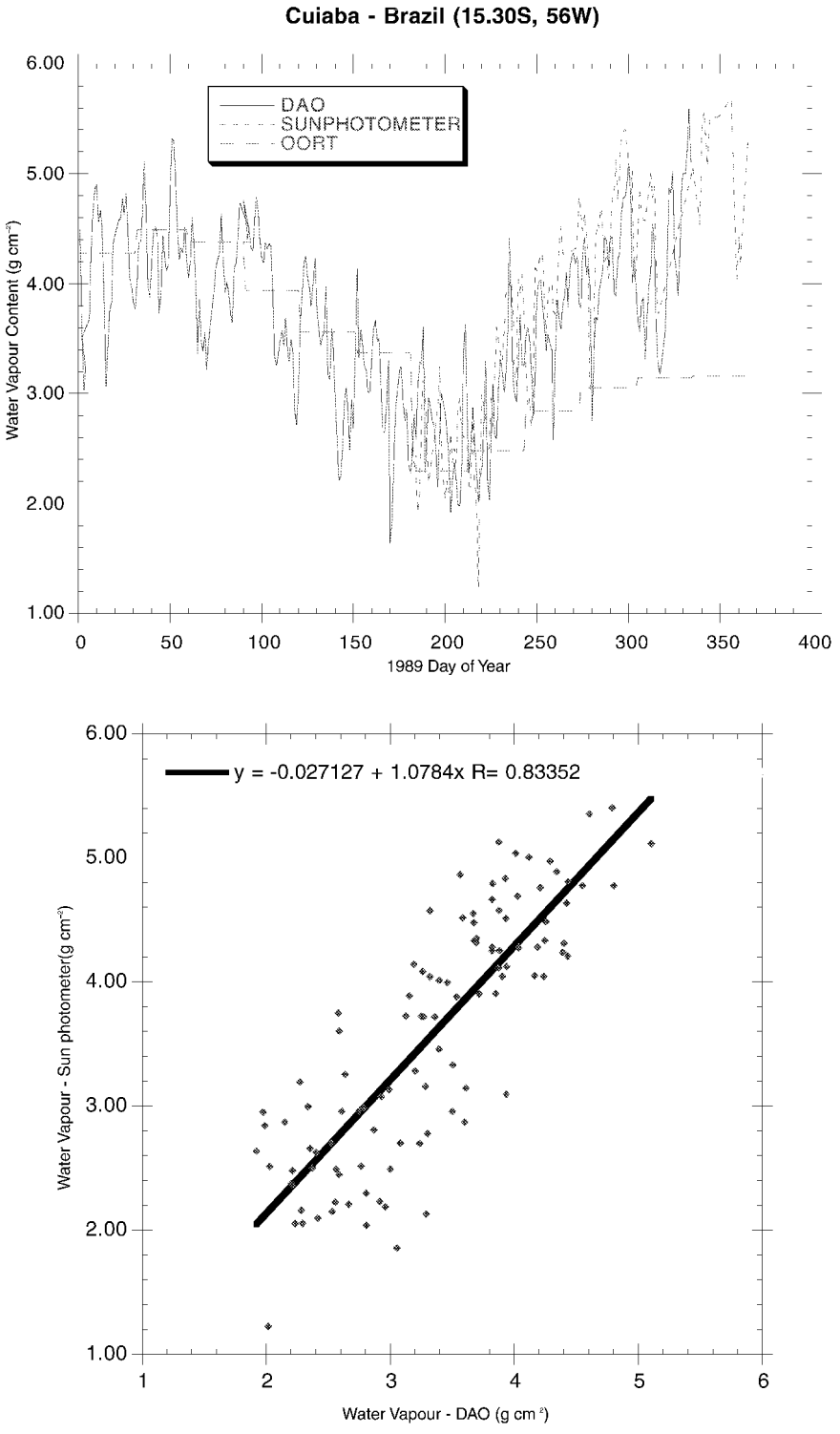

Figure 8. Correlation between water vapour content from DAO and Sun photometer measurements over Cuiaba (Brazil). Oort (1983) climatology values are also shown.

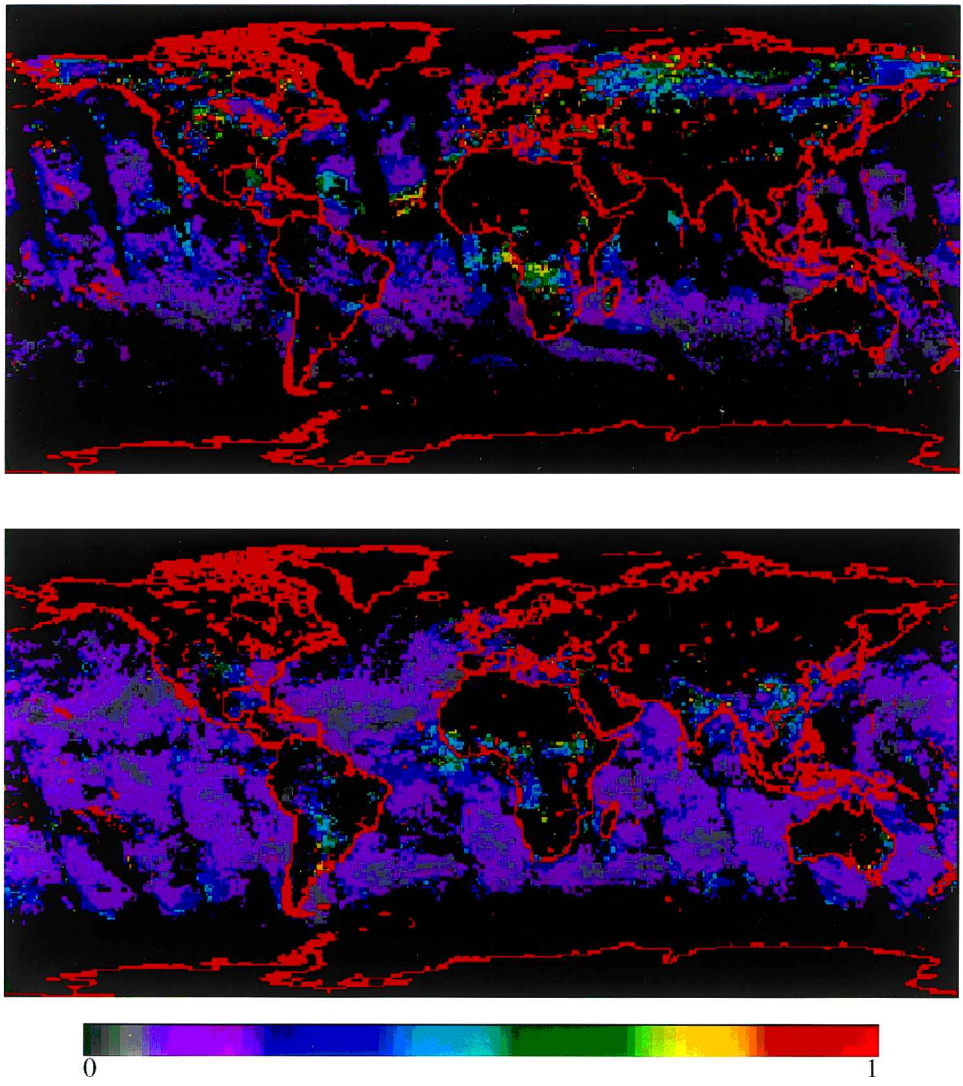

Figure 9. Aerosol optical thickness derived from AVHRR for 1 July and 29 November 1989.

et al. 1998, Wolfe *et al.* 1998). In this approach data are binned without being resampled and the spatial location of each IFOV relative to the binning grid is retained. This gridding method enables a data base of multiple observations from successive satellite overpasses to be accumulated and analysed, for example for multi-temporal compositing.

2.7. *Compositing*

Temporal compositing is used where more than one observation is available for a given grid cell. This takes place for daily products in areas where orbital overlap occurs, which is especially marked in polar latitudes, or when creating multi-day products. In addition to simplifying the data analysis aspect by selecting only one observation per grid cell, this technique results in a considerable reduction in the

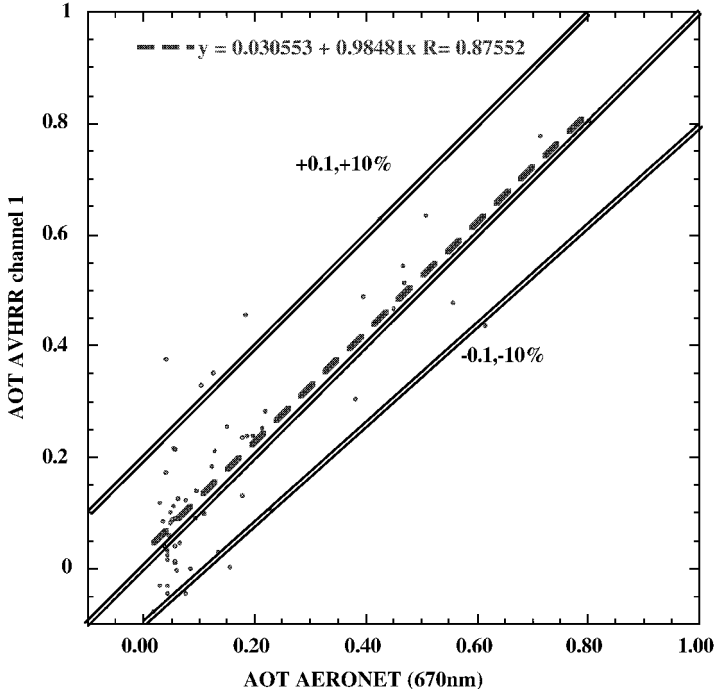

Figure 10. Retrieved versus measured aerosol optical thickness (AOF) over land for October 1997.

data volume of the generated products. It is also widely used to increase the opportunity for cloud free observations and to reduce atmospheric contamination (Holben 1986, Roy 1997). The AVHRR Land Pathfinder II implementation of the compositing procedure takes advantage of the cloud mask generated in the cloud screening step. In the compositing process a lower priority is assigned to observations that were determined to be cloudy.

Different applications benefit from different compositing methods, for example, Roy (1997) notes that compositing by a selection based on maximum NDVI over forest will yield higher NDVI values with lower variance than a selection based on maximum surface temperature, whereas, for the same area, a selection based on maximum surface temperature yields higher surface temperature values with lower variance. To enable the generation of products composited differently, a set of three compositing methods was implemented in the AVHRR Land Pathfinder II processing chain. The set is as follows.

(a) Selecting the observation producing the maximum NDVI value (MaxNDVI) is most commonly used with AVHRR land data (Holben 1986). Clouds over land and atmospheric components (see table 2) tend to reduce the NDVI value, which means that cloud-free and clear pixels will be preferentially selected. The main disadvantages of this method are the selection of cloudy observations over water bodies, the angular bias introduced by preferentially selecting observations from the forward scattering direction (Gutman 1991, Cihlar *et al.* 1994), and its unsuitability for application to individual bands where artifacts due to the selection of neighbouring pixels with different

illumination and viewing geometry are introduced (D'Iorio *et al.* 1991, Cihlar *et al.* 1994).

(b) Selecting the observation producing the minimum reflectance value from Channel 1 (MinCh1) offers a similar advantage as the MaxNDVI criterion for cloud clearing and can be applied equally over land and water. The main disadvantage of this technique is that it is very sensitive to cloud shadow. Cloud shadow should be carefully screened prior to using this approach (see §2.4).

(c) Selecting the observation producing the maximum brightness temperature from channels 4 or 5 (MaxT4 or MaxT5) can be used for compositing the thermal infrared bands. When evaluated over Canada, Cihlar *et al.* (1994) found that this method performed poorly at the extremes of the growing season where partially cloudy areas seemed to have a similar temperature to Sun-illuminated areas.

All of the above mentioned single-step compositing methods can be preceded with a test to limit the preferred range of the sensor viewing angles and hence form a two-step compositing method. For instance, this feature allows one to give higher priority to observations that occur close to nadir and fall within a range of viewing angles preset by the user.

Figure 11 gives an example of products generated for the same area and time period using three different temporal compositing approaches.

3. Products

The products generated by the AVHRR Land Pathfinder II processing system include surface reflectance, brightness temperature, NDVI and active fires. A brief description of these products and some examples are now given.

3.1. *Surface reflectance*

The surface reflectance products are generated from the visible (channel 1), near-infrared (channel 2) and mid-infrared (channel 3) bands. The visible and near infrared channels do not generally include any emissive contribution from the surface. For these two bands, the surface reflectance is computed as follows.

(1) Digital counts are converted into radiance using the calibration method described in §2.3.1.

(2) Radiance is converted into top of the atmosphere (TOA) reflectance:

$$\rho_{\mathrm{TOA}} = L/(\mu_{\mathrm{s}} \cdot d_{\mathrm{sol}}) \tag{5}$$

where μ_{s} is the cosine of the solar zenith angle and d_{sol} is an Earth–Sun distance correction factor that depends on the day of year.

(3) The TOA reflectance is corrected for atmospheric effects using the procedure described in §2.5 to obtain surface reflectance.

The response in the mid-infrared channel (channel 3) consists of a mix of reflective and emissive components, which makes the computation of the surface reflectance more complex. The method used to compute the mid-infrared reflectance was developed by Roger and Vermote (1998). The equations used to compute the

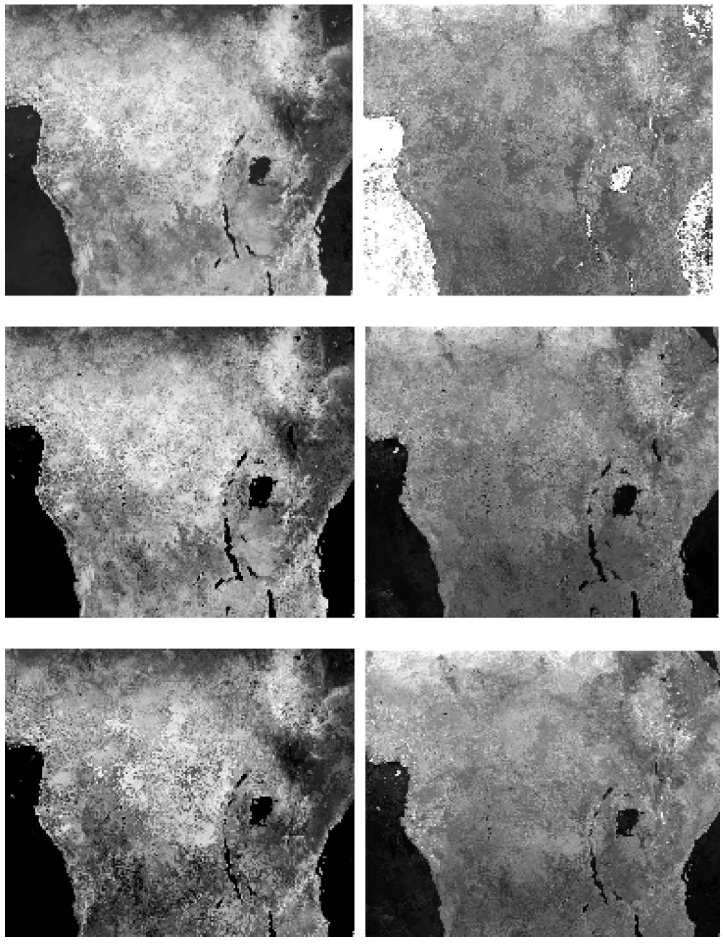

Figure 11. Illustration of the use of different compositing techniques: an NDVI (left column) and near-infrared reflectance (right column) monthly composites for July 1989 generated using maximum NDVI (row 1), minimum channel 1 (row 2) and maximun channel 4 (row 3).

reflectance from channel 3 are:

$$\text{over ocean} \quad \rho_3 = \pi[R_3^{\mathrm{m}} - R_3^{\mathrm{e}}]/[E_3^{\mathrm{s}} \cos(\theta_{\mathrm{s}})\tau_3(\theta_{\mathrm{s}})\tau_3(\theta_{\mathrm{v}})] \tag{6}$$

$$\text{and over land} \quad \rho_3 = \pi[R_3^{\mathrm{m}} - R_3^{\mathrm{e}}]/[E_3^{\mathrm{s}} \cos(\theta_{\mathrm{s}})\tau_3(\theta_{\mathrm{s}})\tau_3(\theta_{\mathrm{v}}) - \pi R_3^{\mathrm{e}}\tau_3(\theta_{\mathrm{v}})] \tag{7}$$

R_3^{m} is the radiance obtained from channel 3 and is equal to $B_3(T_3^{\mathrm{m}})$ with B_3 being Planck's spectral radiance function and T_3^{m} being the brightness temperature obtained from the total channel 3 response. R_3^{e} is the spectral radiance from the emissive component of channel 3 and is equal to $B_3(T_3^{\mathrm{e}})$ with T_3^{e} being an approximation of the brightness temperature obtained from the emissive part of channel 3. It is expressed as a second degree polynomial of the difference between the brightness temperatures from channels 4 and 5 ($T4$–$T5$), the coefficients of which are a function of the emissivity in channels 4 and 5 (Roger and Vermote 1998). E_3^{s} is the spectral exoatmospheric irradiance and τ_3 is the gaseous transmittance in channel 3. In the AVHRR Land Pathfinder II processing, the DAO integrated water vapour field was

used in the computation of this function for atmospheric transmission correction instead of the split window technique as suggested by Roger and Vermote (1998).

The surface reflectance products are scaled to a 16-bit word by multiplying them by a factor of 10 000. A quality bit is also set in the QC flag when the product is out of range.

Figure 12 shows an example of the surface reflectance product. It represents a false colour image generated for the month of January 1989 where data were composited using the minimum channel 1 criterion. The blue band contains the surface reflectance from channel 1, the green band contains channel 2 and the red band contains channel 3. In this configuration, vegetated areas will be displayed as green and non-vegetated areas as white. The blue colour in the northern latitudes is due to snow cover. The blue colour over the Australian desert demonstrates the limitation of use of the AVHRR mid-infrared channel which is expected to saturate at around 327.5 K for NOAA-11 (Robinson 1991).

3.2. *Brightness temperature*

Brightness temperature in the mid-infrared (channel 3) and thermal (channels 4 and 5) bands are computed by converting the digital counts in thermal radiances using the calibration method described in §2.3.2 where account is taken of the nonlinearity of the sensor in channels 4 and 5. The radiances are then converted into temperatures by using the inverse of Planck's radiation equation:

$$T = C_2 v / \log(1 + C_1 v^3 / L) \tag{8}$$

where T is the brightness temperature in K, L is the thermal radiance in milliwatts/(m^2 steradians cm^{-1}), v is the central wavenumber in cm^{-1}, $C_1 = 1.1910659\text{E-}5$ milliwatts/(m^2 steradians cm^{-4}) and $C_2 = 1.438833$ cm K.

Table 4 lists, for different satellites, the central wavenumber used for the three channels as a function of the temperature range.

The brightness temperature product is scaled to a 16-bit word by multiplication by ten and a quality bit is set if the product is not within the valid range.

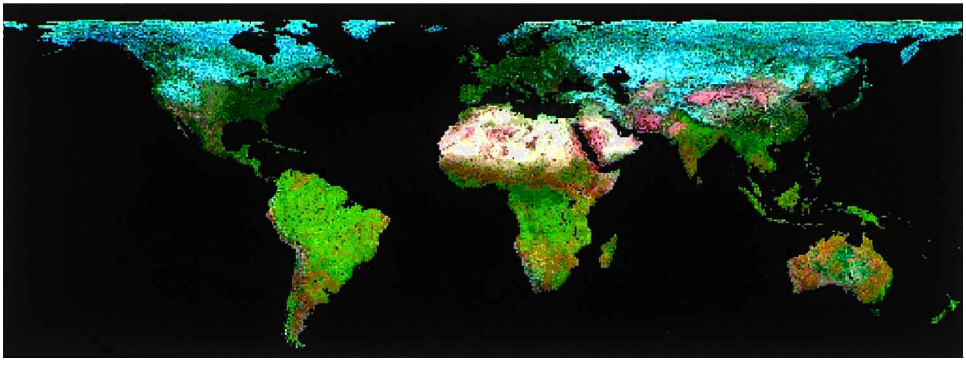

Figure 12. False RGB composite ($R = 3.75\,\mu$m (ch3 reflectance), $G = 0.87\,\mu$m (ch2), $B = 0.670\,\mu$m (ch1)) for January 1989. The monthly composite was generated by selecting the pixels with minimum response in channel 1.

Table 4. Central wavenumbers (in cm^{-1}) used in the conversion of thermal radiance into brightness temperature.

T range (K)	NOAA-7			NOAA-9			NOAA-11		
	ch3	ch4	ch5	ch3	ch4	ch5	ch3	ch4	ch5
180–225	2670.30	926.20	840.100	2670.93	928.50	844.41	2663.50	926.80	837.75
225–275	2670.30	926.80	840.500	2674.81	929.02	844.80	2668.15	927.34	838.08
> 275	2671.90	927.22	840.872	2678.11	929.46	845.19	2671.40	927.80	838.40

3.3. *NDVI*

The NDVI is computed from channel 1 and 2 surface reflectances as follows:

$$\mathrm{NDVI} = (\rho_2 - \rho_1)/(\rho_2 + \rho_1) \tag{9}$$

The NDVI is a key remote sensing observation related to several important biospheric properties including the proportion of photosynthetically absorbed radiation and leaf area index. This variable can be readily calculated from the reflectances provided as part of the product, but is included to assist users with more limited computational facilities.

3.4. *Active fires*

The AVHRR active fire detection algorithm used in the AVHRR Land Pathfinder II code was developed specifically for global 1 km application, using bands 3 and 4 (Kendall *et al.* 1996, Giglio *et al.* 1998). For daytime scenes band 2 is also used to eliminate false detection caused by highly reflective surfaces. Land/water and cloud masks are used to exclude water and cloud pixels from processing.

The algorithm employs several threshold tests to eliminate obvious non-fire pixels. If these tests are passed, neighbouring background pixels are characterized statistically, and several relative tests are then performed to identify a fire pixel. If these additional tests are passed the pixel is classified as 'fire', otherwise it is classified as 'non-fire'.

The AVHRR Land Pathfinder II fire product consists of a 3-bit pixel class (missing, water, cloud, non-fire, unknown and fire); a 2-bit confidence estimate for each fire pixel, and a 11-bit quality assurance (QA) value are included for every pixel. Each QA value contains eight individual QA fields. A full description of the algorithm may be found in the work of Giglio *et al.* (1998). Figure 13 shows an example of the active fires product derive from 1 km AVHRR data.

4. Evaluation

In order to asses the quality of the products generated by the AVHRR Land Pathfinder II code, a preliminary test data set consisting of one year of global 8 km data and a set of time series over different land cover types was created. The product evaluation process includes visual inspection of the generated data to ensure proper registration of the data and the absence of dropped or bad scan lines. Another important component of the evaluation activity is the comparison between the AVHRR Land Pathfinder II products and other existing data sets such AVHRR Pathfinder 1 data set (James and Kalluri 1994), FASIR (Fourier Adjustment, Solar zenith angle correction, Interpolation and Reconstruction of NDVI) (Los *et al.* 1994) and LASUR (Berthelot *et al.* 1996).

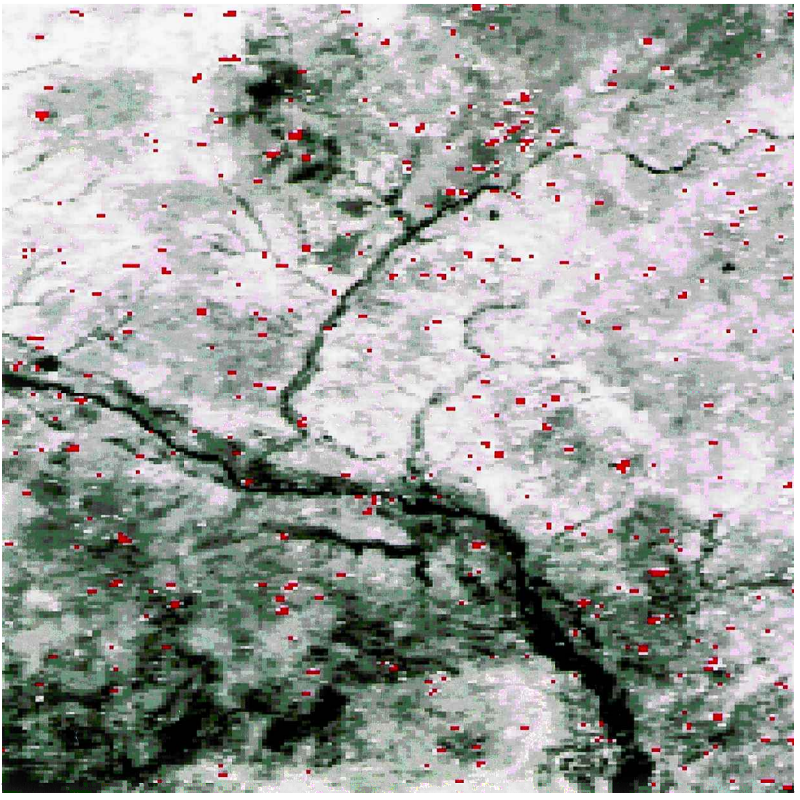

Figure 13. Example of active fires detection algorithm over dry tropical savanna. Product derived from NOAA-11 data for 14 January 1993 over the Ivory Coast, West Africa (Giglio *et al.* 1998).

The first results were presented by Ouaidrari *et al.* (1997) where the AVHRR Land Pathfinder II NDVI product was compared to FASIR and LASUR data sets over eight sites representative of major cover types. Examples of those results are included in figure 14. Generally, this figure shows good agreement between the AVHRR Land Pathfinder II NDVI and the LASUR NDVI for the different sites. Some differences are observed, though the Pathfinder II data exhibit less perturbations due to cloud contamination than do the LASUR data. Other differences, such as those observed in the 'broad leaf deciduous' case, are mainly due to the use of ozone and water vapour climatology in the atmospheric correction step of LASUR data whereas more realistic estimates (based on TOMS measurements for ozone and DAO assimilated data for water vapour) are used in the Pathfinder II atmospheric correction process.

Two test cases were used to compare 10-day composited red and near-infrared reflectances from the AVHRR Land Pathfinder II and the AVHRR Pathfinder version 1 data set. The first case represents a soil site selected over the Saharan desert and covers a rectangle with an upper left corner (UL) defined by (25° N, 10° W) and a lower right corner (LR) defined by (17° N, 30° E). The second case represents a vegetation site over Central Africa and covers a rectangle defined by UL = (7° N, 12° E) and LR = (2° S, 32° E). Histograms of the red and near-infrared

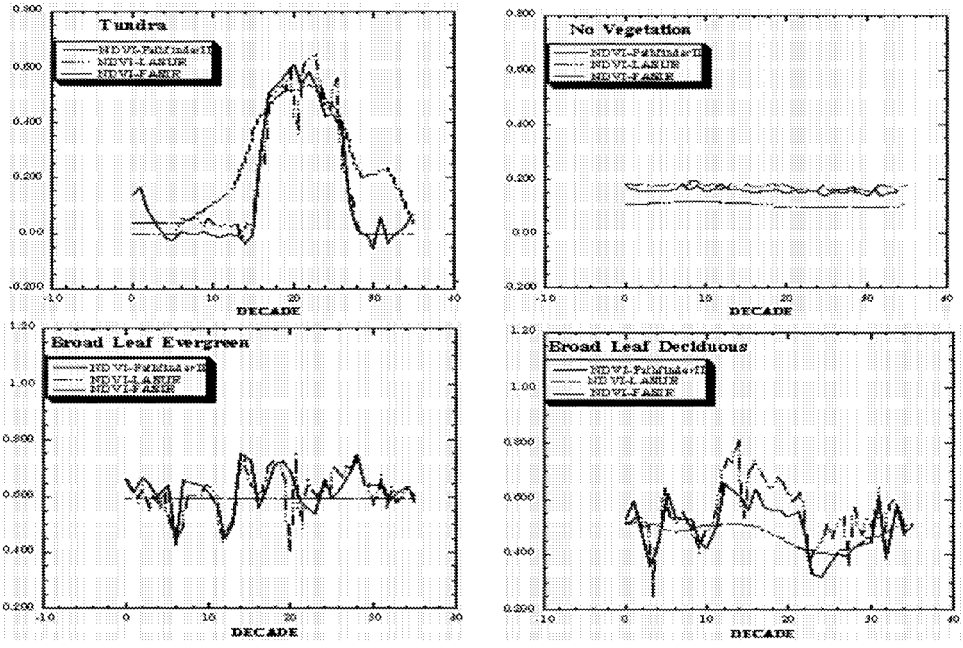

Figure 14. NDVI time series for four land cover types (tundra, no vegetation, broad leaf evergreen and broad leaf deciduous) from Pathfinder II, LASUR and FASIR data sets.

reflectance for the period 1–10 July 1989 obtained from both data sets are ploted in figure 15. The histograms for both sites show a larger difference in channel 2 reflectance than that in channel 1. This is due to the absence of water vapour correction in the AVHRR Pathfinder 1 product. The lack of water vapour correction leads to an underestimating of the NDVI in both cases.

5. Conclusions

The development of stable long-term data records for land studies is a high priority for the global change research community. The AVHRR provides the longest record of global-scale remotely sensed data for land studies. The AVHRR instrument series with NOAA K, L, M will extend the AVHRR data record for another ten to fifteen years. However, the creation of an internally consistent data set amongst the AVHRR sensors and the generation of a consistent record with new sensors such as the Earth Observing System's Moderate Resolution Imaging Specrometer (EOS MODIS) will continue to require a considerable processing effort for some years to come.

The Pathfinder II code represents the most recent advance in AVHRR data processing for land studies and provides an improvement over the Pathfinder 1 processing. The demonstrated improvements over existing AVHRR processing algorithms using a significant sample of the data record now indicates the need to apply the AVHRR Land Pathfinder II code to reprocess the existing AVHRR data record, with the objective of making the AVHRR Land Pathfinder II code generally available at the end of the project.

In several aspects the AVHRR Land Pathfinder II code includes several characteristics of those applied in the MODIS processing chain and hence provides an early

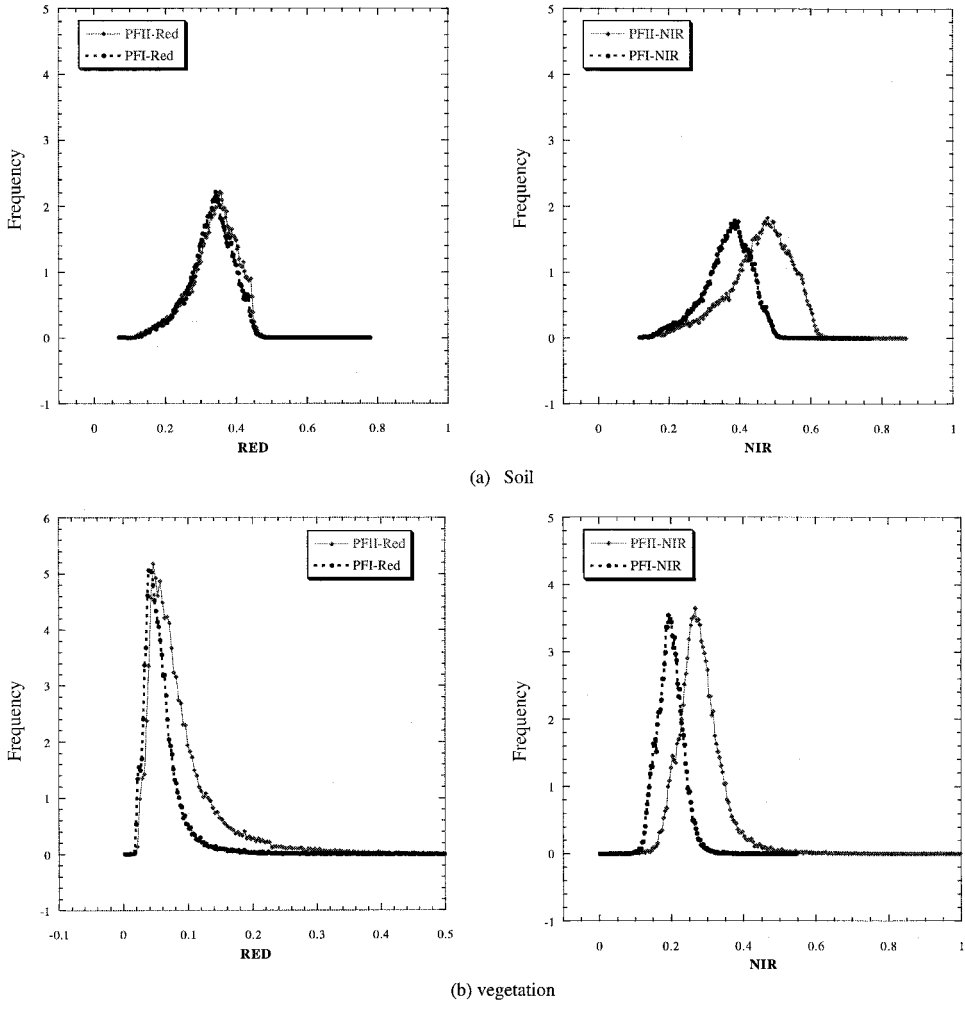

Figure 15. Red and near-infrared reflectance histograms computed from 10-day composites from AVHRR Land Pathfinder II (PFII) and AVHRR Pathfinder I (PFI) data sets for soil (*a*) and vegetation (*b*).

test of MODIS data processing (Running *et al.* 1994, Justice *et al.* 1998). In particular, the AVHRR Land Pathfinder II L2G binning, initially designed as part of the MODIS product development effort, will enable experimentation with compositing techniques prior to the launch of MODIS (Wolfe *et al.* 1998). The AVHRR Land Pathfinder II code will facilitate inter-comparisons between AVHRR and MODIS data. Similarly, L2G will facilitate an inter-comparison and fusion of AVHRR data with other moderate resolution data sets such as those from Sea-viewing Wide Field-of-view Sensors (SeaWiFs) and SPOT Vegetation.

Acknowledgments

This project was funded by NASA Grant NAGW4790. We would like to thank James Ray and Damianos Karakos for their efforts in the development and imple-

mentation of the processing system, and Dr Hassan Ouaidrari for his help in the evaluation of generated products.

7. References

Baldwin, D., and Emery, W. J., 1995, Spacecraft attitude variations of NOAA-11 inferred from AVHRR imagery. *International Journal of Remote Sensing*, **16**, 531–548.

Berthelot, B., Adam, S., Kergoat, L., Cabot, F., Dedieu, G., and Maisongrande, P., 1996, Global weekly LAnd SUrface Reflectances—LASUR 1989–1990, Version 0, May 1996. 2 CD-ROMs. CESBIO. Toulouse, France.

Brush, R. J. H., 1982, A real time data retrieval system for images from polar orbiting satellites. Ph.D. Thesis, University of Dundee, Scotland.

Chandrasekhar, S., 1960, *Radiative Transfer* (New York: Dover).

Cihlar, J., Manak, D., and D'Iorio, M., 1994, Evaluation of compositing algorithms for AVHRR data over land. *IEEE Transactions on Geoscience and Remote Sensing*, **32**, 427–437

Cracknell, A. P., 1997, The advanced very high resolution radiometer (AVHRR) (London: Taylor and Francis).

D'Iorio, M. A., Cihlar, J., and Morasse, C. R., 1991, Effect of the calibration of AVHRR data on the normalized difference vegetation index and compositing. *Canadian Journal of Remote Sensing*, **17**, 251–262.

DeFries, R. S., and Townshend, J. R. G., 1994, NDVI-derived land cover classifications at a global scale. *International Journal of Remote Sensing*, **15**, 3567–3586.

Eidenshink, J. C., and Faundeen, J. L., 1994, The 1 km AVHRR global land data set: first stages in implementation. *International Journal of Remote Sensing*, **15**, 3443–3462.

GCTP, 1982, Software Documentation for GCTP General Cartographic Transformation Package: National Mapping Program Technical Instructions. U.S. Geological Survey, National Mapping Division, Sioux Falls, South Dakota, USA.

Giglio, L., Kendall, J. D., and Justice, C. O., 1999, Evaluation of global fire detection algorithms using simulated AVHRR infrared data. *International Journal of Remote Sensing*, **20**, 1947–1985.

Gutman, G. G., 1991, Vegetation indices from AVHRR: an update and future prospects. *Remote Sensing of Environment*, **35**, 121–136.

Herman, J. R., Bhartia, P. K., Krueger, A. J., McPeters, R. D., Wellemeyer, C. G., Seftor, C. J., Jaross, G., Schlesinger, B. M., Torres, O., Labow, G., Byerly, W., Taylor, S. L., Swissler, T., Cebula, R. P., and Gu, X., 1996, Meteor-3 Total Ozone Mapping Spectrometer (TOMS) Data Products User's Guide. NASA Reference Publication 1393, National Aeronautics and Space Administration, Washington, DC, USA.

Ho, D., and Asem, A., 1986, NOAA AVHRR image referencing, *International Journal of Remote Sensing*, **7**, 895–904.

Holben, B. N., 1986, Characteristics of maximum-value composite images for temporal AVHRR data. *International Journal of Remote Sensing*, **7**, 1435–1445.

Holben, B. N., Eck, T. F., Slutsker, I., Tanrè, D., Buis, J. P., Setzer, A., Vermote, E. F., Reagan, J. A., Kaufman, Y. J., Nakajima, T., Lavenu, F., Jankowiak, I., and Smirnov, A., 1998, AERONET-A Federated Instrument Network and Data Archive for Aerosol Characterization. *Remote Sensing of Environment*, **66**, 1–16.

Holben, B. N., Kaufman, Y. J., and Kendall, J. D., 1990, NOAA-11 AVHRR visible and near-IR inflight calibration. *International Journal of Remote Sensing*, **11**, 1511–1519.

James, M. E., and Kalluri, S. N. V., 1994, The Pathfinder AVHRR land data set: an improved coarse resolution data set for terrestrial monitoring. *International Journal of Remote Sensing*, **15**, 3347–3363.

Justice, C. O., and Townshend, J. R. G., 1994, Data sets for global remote sensing: lessons learnt. *International Journal of Remote Sensing*, **15**, 3621–3639.

Justice, C. O., Vermote, E., Townshend, J., DeFries, R., Roy, D., Hall, D., Salomonson, D., Privette, J., Riggs, G., Strahler, A., Lucht, W., Myneni, R., Knjazihhin, Y., Running, S., Nemani, R., Wan, Z., Huete, A., Van Leeuwen, W., Wolfe, R., Giglio, L., Muller, J. P., Lewis, P., and Barnsley, M., 1998, The

Moderate Resolution Imaging Spectroradiometer (MODIS): land remote sensing for global change research. *IEEE Transactions on Geoscience and Remote Sensing*, **36**, 1228–1249.

Kendall, J. D., Justice, C. O., Dowty, P. R., Elvidge, C. D., and Goldammer, J. G., 1996, Remote sensing of fires in Southen Africa during the SAFARI 1992 Campaign. In *Fire in Southern Africa Savannas: Ecological and Atmospheric Perpectives*, edited by B. W. van Wilgen, M. O. Andreae, J. G. Goldammer and J. A. Lindesay (Johannesburg: Witwatersand University Press), pp. 89–130

Kidwell, K. B., 1997, NOAA Polar Orbiter Data Users Guide (TIROS-N, NOAA-6, NOAA-7,NOAA-8,NOAA-9,NOAA-10,NOAA-11, NOAA-12, NOAA-13 AND NOAA-14). National Oceanic and Atmospheric Administration, Rockvilt, MD, USA.

Laporte, N., Justice, C., and Kendall, J., 1995, Mapping the dense humid forest of Cameroon and Zaire using AVHRR satellite data. *International Journal of Remote Sensing*, **16**, 1127–1145

London, J., Bojkov, D. R., Oltmans, S., and Kelly, J. L., 1976, Atlas of the Global Distribution of the Total Ozone July 1957–June 1967. Technical Note, NCAR/TN/113 + STR, The National Center for Atmospheric Research (NCAR), Boulder, CO, USA.

Los, S. O., Justice, C. O., and Tucker, C. J., 1994, A global $1° \times 1°$ NDVI data set for climate studies derived from the GIMMS continental NDVI data. *International Journal of Remote Sensing*, **15**, 3493–3518.

Loveland, T. R., and Belward, A. S., 1997, The IGBP-DIS global 1 km land cover data set, DISCover: first results. *International Journal of Remote Sensing*, **18**, 3291–3295.

Maiden, M. E., and Greco, S., 1994, NASA's Pathfinder data set programme: land surface parameters. *International Journal of Remote Sensing*, **15**, 3333–3345.

McPeters, R. D., Krueger, A. J., Bhartia, P. K., Herman, J. R., Oakes, A., Ahmad, Z., Cebula, R. P., Schlesinger, B. M., Swissler, T., Taylor, S. L., Torres, O., and Wellemeyer, C. G., 1993, Nimbus-7 Total Ozone Mapping Spectrometer (TOMS) Data Products User's Guide. *NASA Reference Publication* 1323, National Aeronautics and Space Administration, Washington, DC, USA.

Moreno, J. F., and Melia, J., 1993, A method for accurate geometric correction of NOAA AVHRR HRPT data. *IEEE Transactions on Geoscience and Remote Sensing*, **31**, 204–226.

Myneni, R. B., Keeling, C. D., Tucker, C. J., Asrar, G., and Nemani, R. R., 1997, Increased plant growth in the northern high latitudes from 1981 to 1991. *Nature*, **386**, 698–702.

Oort, A. H., 1983, Global atmospheric circulation statistics: 1958–1973. *NOAA Professional Paper 14*, NOAA, Rockville, MD, USA.

Ouaidrari, H., Vermote, E., El Saleous, N., and Roy, D., 1997, AVHRR Pathfinder II data set: evaluation and improvements. *Proceedings of Seventh International Symposium on Physical Measurements and Signatures in Remote Sensing*, edited by G. Guyot and T. Phu (Rotterdam: Balkema). 7–11 April 1997, Courchevel, France.

Rao, C. R. N., 1993a, Degradation of the visisble and near-infrared channels of the Advanced High Resolution Radiometer on the NOAA-9 spacecraft: assessment and recommendations. *NOAA Technical Report NESDIS-70*, NOAA/NESDIS, Washington, DC, USA.

Rao, C. R. N., 1993b, Non-linearity corrections for the thermal infrared channels of the Advanced High Resolution Radiometer: assessment and recommendations. *NOAA Technical Report NESDIS-69*, NOAA/NESDIS, Washington, DC, USA.

Robinson, J. M., 1991, Fire from space: global fire evaluation using infrared remote sensing. *International Journal of Remote Sensing*, **12**, 3–24.

Roger J. C., and Vermote, E. F., 1998, A method to retrieve the reflectivity signature at 3.75 mm from AVHRR data. *Remote Sensing of Environment*, **64**, 103–114

Rosborough, G. W., Baldwin, D. G., and Emery, W. J., 1994, Precise AVHRR navigation. *IEEE Transactions on Geoscience and Remote Sensing*, **32**, 644–657.

Roy, D. P., 1997, Investigation of the maximum normalized vegetation index (NDVI) and the maximum surface temperature (T_s) AVHRR compositing procedures for the extraction of NDVI and T_s over forest. *International Journal of Remote Sensing*, **18**, 2383–2401.

Running, S. W., Justice, C. O., Salomonson, V., Hall, D., Barker, J., Kaufmann, Y. J.,

Strahler, A. H., Huete, A. R., Muller, J. P., Vanderbilt, V., Wan, Z. M., Teillet, P. M., and Carneggie, D., 1994, Terrestrial remote sensing science and algorithms planned for EOS MODIS. *International Journal of Remote Sensing*, **15**, 3587–3620.

Schubert, S. D., Rood, R. B., and Pfaendtner, J., 1993, An assimilated data set for earth science applications. *Bulletin of the American Meteorological Society*, **74**(12), 2331–2342.

Sellers, P. J., Tucker, C. J., Collatz, G. J., Los, S. O., Justice, C. O., Dazlich, D. A., and Randall, D. A., 1994, A global 1° by 1° NDVI data set for climate studies. Part 2: the generation of global fields of terrestrial biophysical parameters from the NDVI. *International Journal of Remote Sensing*, **15**, 3519–3545.

Simpson, J. J., and Gobat, J. I., 1996, Improved cloud detection for daytime AVHRR scenes over land. *Remote Sensing of Environment*, **55**, 21–49

Stowe, L. L., Davis, P., and McClain, E. P., 1995, Evaluating the CLAVR (CLouds from AVHRR) phase-I cloud cover experimental product. *Advances in Space Research*, **16**, 21–24

Stowe, L. L., McClain, E. P., Carey, R., Pellegrino, P., Gutman, G. G., Davis, P., Long, C., and Hart, S., 1991, Global Distribution of Cloud Cover derived from NOAA/AVHRR operational Satellite Data. *Advances in Space Research*, **11**, 51–54.

Stowe, L. L., Ignatov, A. M., and Singh, R. R., 1997, Development, validation, and potential enhacement to the second generation operational aerosols product at the National Environmental Satellite, Data, and Information Service of the National Oceanic and Atmospheric Administration. *Journal of Geophysical Research*, **102**, 16 923–16 934.

Tanrè, D., Holben, B. N., and Kaufman, Y. J., 1992, Atmospheric correction algorithm for NOAA-AVHRR products: theory and application. *IEEE Transactions on Geoscience and Remote Sensing*, **30**, 231–248.

Teillet, P. M., Slater, P. N., Ding, Y., and Santer, R. P., 1990, Three methods for the absolute calibration of the NOAA AVHRR sensors in-flight. *Remote Sensing of Environment*, **31**, 105–120.

Townshend, J. R. G., 1994, Global data sets for land applications from the Advanced Very High Resolution Radiometer: an introduction. *International Journal of Remote Sensing*, **15**, 3319–3332.

Townshend, J. R. G., Justice, C. O., Skole, D., Malingreau, J.-P., Cihlar, J., Teillet, P., Sadowski, F., and Ruttenberg, S., 1994, The 1 km resolution global data set: needs of the International Geosphere Biosphere Programme. *International Journal of Remote Sensing*, **15**, 3417–3441.

Tucker, C. J., Newcomb, W. W., and Dregne, A. E., 1994, AVHRR data sets for determination of desert spatial extent. *International Journal of Remote Sensing*, **15**, 3519–3545.

Vermote, E., El Saleous, N., and Holben, B., 1996, Aerosol retrieval and atmospheric correction. In *Advances in the Use of NOAA AVHRR Data for Land Applications* (Dordrecht: Kluwer).

Vermote, E., and Kaufman, Y. J., 1995, Absolute calibration of AVHRR visible and near infrared channels using ocean and cloud views. *International Journal of Remote Sensing*, **16**, 2317–2340.

Vermote, E. F., and Tanrè, D., 1992, Analytical expressions for radiative properties of planar Rayleigh scattering media including polarization contribution. *Journal of Quantitative Spectroscopy and Radiative Transfer*, **47**, 305–314.

Vermote, E. F., Tanrè, D., Deuzè, J. L., Herman, M., and Morcrette, J. J., 1997, Second Simulation of the Satellite Signal in the Solar Spectrum: an overview. *IEEE Transactions on Geoscience and Remote Sensing*, **35**, 675–686.

Weinreb, M. P., Hamilton, G., Brown, S., and Koczor, R. J., 1990, Nonlinearity corrections in calibration of Advanced Very High Resolution Radiometer infrared channels. *Journal of Geophysical Research*, **95**, 7381–7388.

Wessel, P., and Smith, W. H. F., 1996, A global, self-consistent, hierarchical, high-resolution shoreline database. *Journal of Geophysical Research*, **101**, 8741–8743

Wolfe, R. E., Roy, D. P., and Vermote, E. F., 1998, The MODIS land data storage, gridding and compositing methodology: level 2 Grid. *IEEE Transactions on Geoscience and Remote Sensing*, **36**, 1324–1338